ACS APPLIED MATERIALS & INTERFACES

Research Article

www.acsami.org

Double Detection of Mycotoxins Based on SERS Labels Embedded Ag@Au Core–Shell Nanoparticles

Yuan Zhao,* Yaxin Yang, Yaodong Luo, Xuan Yang, Manli Li, and Qijun Song*

The Key Lab of Food Colloids and Biotechnology, Ministry of Education, School of Chemical and Material Engineering, Jiangnan University, Wuxi, Jiangsu 214122, People's Republic of China

Supporting Information

ABSTRACT: A sensitive surface-enhanced Raman scattering (SERS) signal dependent double detection of mycotoxins is achieved for the first time, without the aid of nucleic acid amplification strategies. SERS labels embedded Ag@Au core–shell (CS) nanoparticles (NPs) as novel SERS tags are successfully prepared through a galvanic replacement-free deposition. SERS tags produce stable and quantitative SERS signal, emerging from the plasmonic coupling at the junction of Ag core and Au shell. SERS tags engineered Raman aptasensors are developed for the double detection of ochratoxin A (OTA) and aflatoxin B1 (AFB1) in maize meal. The limits of detection (LODs) are as low as 0.006 ng/mL for OTA and 0.03 ng/mL for AFB1. The developed protocol can be extended to a large set of different SERS tags for the sensitive detection of multiple targets that possess different lengths of aptamers.

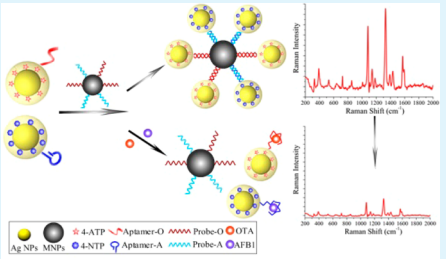

KEYWORDS: *embed, mycotoxins, double detection, Ag core, SERS*

1. INTRODUCTION

Mycotoxins are toxic secondary metabolites released by fungi which easily grow on contaminated cereals. A majority of mycotoxins are carcinogenic, mutagenic, and hepatotoxic.[1−3] In particular, ochratoxin A (OTA) and aflatoxin B1 (AFB1) are the ones most frequently existing in cereal samples.[1,2] Several techniques were explored for the detection of OTA and AFB1, involving chromatographic methods, fluorescence analysis, and immunoassay (Table 1).[1,4−7] However, the requirements of expensive instruments, trained personnel, and time-consuming procedures limit the application of chromatographic methods.[6,8,9] Fluorescence signal is easily interfered with by oxygen, humidity, and foreign species.[3] Immunoassay is dependent on the susceptible antibody, and its efficiency is hindered by the complex and repetitive protocols.[6,7,10] Interestingly, aptasensors featured with the advantages of excellent specificity have considerable potential for the detection of mycotoxins.[8,10] Aptamers of OTA and AFB1 (denoted as aptamer-O and aptamer-A) are reported in succession and exhibit favorable bioaffinity toward targets. The dissociation constants (K_d) are 50 nM for aptamer-O and 75 nM for aptamer-A, respectively.[1,5,9,11−14] Even though aptasensors can detect mycotoxins at pictogram and even femtogram levels, most of them need the help of amplification strategies.[8−10,15,16] The amplification techniques require extra complex operations and concomitantly induce false-positive results. It is of urgent necessity to develop an accurate, sensitive, and DNA-amplification-free method for multiplex hidden mycotoxin detection.

Surface-enhanced Raman scattering (SERS), featured with narrow bandwidth and characteristic molecular fingerprint spectra, has emerged as a sensitive technique with the ability to detect multiple analytes simultaneously.[17−19] Numerous SERS assemblies had been developed for the detection of DNA, disease biomarkers, proteins, and heavy metal ions.[20−24] SERS signal of assemblies is highly dependent on the plasmonic coupling at the gaps of two or more neighboring metal nanoparticles (NPs) where the electromagnetic field is strongest.[25,26] However, the long length of aptamers for AFB1 (50 bp) and OTA (36 bp) would produce a large gap between NPs, resulting in a weak SERS signal for assemblies.[8−10,27] SERS tags by embedding Raman labels in the junction of core and shell exhibit amplified SERS signal, without the precise control of the gap size between neighboring NPs. The fabrication of multiplex and strong SERS tags permits more rapid and high-throughput detection of mycotoxins than that obtained with existing methods.[28]

A tremendous amount of effort had been devoted to maximizing the SERS enhancement factor. Various SERS tags were prepared, involving Au@SiO_2 NPs, Ag@SiO_2 NPs, MNPs@Ag@silica (MNPs, magnetic nanoparticles), MNPs@silica@Ag@silica, Fe_3O_4@TiO_2@Au NPs, and so on.[22,29−34] Alternatively, SERS tags composed of a bimetallic plasmonic nucleus and coating layer exhibit unique localized surface plasmon resonance (LSPR) which is responsible for the amplification of Raman signal.[35−37] Fortunately, Ag possesses the best plasmonic enhancement,[23,40,41] and Au featured with an excellent biocompatibility can serve as an external coating on the Ag core, to prevent the oxidation of Ag and improve the stability.[38] However, a galvanic reaction occurs instantaneously

Received: June 23, 2015
Accepted: September 18, 2015
Published: September 18, 2015

DOI: 10.1021/acsami.5b07804
ACS Appl. Mater. Interfaces 2015, 7, 21780−21786

Table 1. Comparison of Limits of Detection (LODs) of Different Assays for OTA and AFB1 Detection

assay	OTA (ng/mL)	AFB1 (ng/mL)	ref
SERS		1.56×10^4	50
SERS		13	51
fluorescent immunoassay		0.2	4
chemiluminescence competitive aptamer assay		0.11	7
SERS-based immunoassay		0.1	52
aptamer-based dipstick assay		0.1	6
electrochemical aptasensors		0.016	27
impedimetric immunosensor		1×10^{-5}	2
real-time quantitative polymerase chain reaction (RT-PCR) based aptasensor[a]		2.5×10^{-5}	10
SERS signal based double detection of mycotoxins	0.006	0.03	this work
aptamer-based evanescent wave all-fiber biosensor	1.2		13
LSPR aptasensor	0.4		5
Raman aptasensor	0.04		14
photonic crystal embedded suspension array	2.5×10^{-4}		1
exonuclease-catalyzed target recycling amplification[a]	6.4×10^{-4}		16
loop-mediated isothermal amplification based electrochemical aptasensor[a]	1.2×10^{-4}		15
rolling circle amplification based electrochemical aptasensor[a]	6.5×10^{-5}		8
RT-qPCR based aptasensor[a]	1×10^{-6}		9

[a]Amplification techniques.

when Ag core mixes with $HAuCl_4$ solution, resulting in the formation of hollow Au NPs, nanoframes, and nanocages.[39−41] It is challenging to fabricate SERS labels embedded solid Ag@Au core−shell (CS) NPs, and it is urgently demanded to exploit the SERS activity of SERS labels embedded solid Ag@Au CS NPs for the application of rapid and multiplex detection of mycotoxins.

This work first fabricates two kinds of SERS labels embedded solid Ag@Au CS NPs through a galvanic replacement-free deposition. The innovative design of Ag core and Au shell ensures a strong plasmonic coupling which greatly amplifies the SERS signal of Raman labels. Au shell prevents Raman labels from leaching out into the medium and increases the chemical stability. SERS labels embedded Ag@Au CS NPs employed as stable and strong SERS tags achieve ultrasensitive double detection of OTA and AFB1 in maize meal. This protocol inspires new designs of SERS for multiple-analyte assay depending on different lengths of aptamers, antibodies, and other recognition systems.

2. EXPERIMENTAL SECTION

2.1. Materials and Reagents. Chloroauric acid ($HAuCl_4$), trisodium citrate, AFB1, OTA, ochratoxin B (OTB), and fumonisin B1 (FB1) were obtained from Sigma-Aldrich. Silver nitrate ($AgNO_3$), sodium borohydride ($NaBH_4$), poly-*N*-vinyl-2-pyrrolidone (PVP), ascorbic acid, $FeCl_3$, sodium acetate, 1-ethyl-3-(3-(dimethylamino)-propyl) carbodiimide (EDC), *N*-hydroxysuccinimide (NHS), ethylene glycol, L-cysteine (L-Cys), bovine serum albumin (BSA), and glutathione (GSH) were all obtained from Sinopharm Chemical Reagent Beijing Co., Ltd. 4-Nitrothiophenol (4-NTP), 4-amino-thiophenol (4-ATP), aflatoxin B2 (AFB2), aflatoxin G1 (AFG1), aflatoxin G2 (AFG2), warfarin, and ochratoxin C (OTC) were obtained from J&K Scientific Ltd. Aptamers and complementary DNA fragments purified by HPLC were obtained from Shanghai Sangon Biological Engineering Technology & Services Co., Ltd. (Table S1, Supporting Information).

2.2. Preparation of SERS Labels Embedded Au@Ag CS NPs and Ag@Au CS NPs. Au NPs and Ag NPs with a diameter of 15 ± 3 nm were synthesized according to the reported literature.[38,42] An amount of 1 mL of Au NPs or Ag NPs was centrifuged at 5400*g* for 10 min. The precipitates were dissolved in 100 μL of ultrapure water. 4-ATP as Raman labels was modified on the surface of the Au NPs and Ag NPs through Au−SH and Ag−SH covalent bonds. The final concentration of 4-ATP was 2 μM. After 12 h, the conjugates were centrifuged at 5400*g* for 10 min to remove the unreacted 4-ATP, and the NPs@4-ATP conjugates were dissolved in ultrapure water.

Au@4-ATP@Ag CS NPs were prepared as follows: An aliquot of 200 μL of 0.1 M PBS solution was mixed with 100 μL of 1% PVP (stabilizer) and 50 μL of 0.1 M ascorbic acid (reducing agent). After stirring for 5 min, 50 μL of 200 nM Au@4-ATP NPs and 100 μL of 2 mM $AgNO_3$ solution were added into the above solution and kept shaking for 3 h in the dark. Finally, the mixtures were centrifuged and the precipitates were dissolved in 50 μL of ultrapure water.

Ag@4-ATP@Au CS NPs were prepared as follows: An amount of 1 mL of 1% PVP was mixed with 100 μL of 100 mM ascorbic acid and 100 μL of 200 mM NaOH solution. After stirring for 5 min, 50 μL of 200 nM Ag@4-ATP NPs and 100 μL of 2 mM $HAuCl_4$ solution were added into the above solution. The next procedures were similar to the steps mentioned above. At the same time, 4-ATP could be replaced by 4-NTP to fabricate Ag@4-NTP@Au CS NPs.

2.3. Immobilization of Aptamers. An aliquot of 50 μL of 200 nM Ag@4-ATP@Au CS NPs and Ag@4-NTP@Au CS NPs were mixed with 10 μM aptamer-O and aptamer-A in 0.5× TBE containing 50 mM NaCl, respectively. The coupling ratio of aptamers to NPs was optimized to 1:1. After 12 h, the mixtures were centrifuged to remove the excess aptamers, and the conjugates were dissolved in 50 μL of ultrapure water.

2.4. Synthesis and Modification of Magnetic Nanoparticles (MNPs). Carboxyl-modified MNPs were synthesized according to previously reported methods.[43] Briefly, 0.6 g of $FeCl_3$ and 0.4 g of trisodium citrate were added into 20 mL of ethylene glycol. After stirring for 30 min, 1.2 g of sodium acetate was added. The mixture reacted at 230 °C for 12 h. MNPs were washed with ethanol solution three times through magnetic separation.

Aminated DNA fragments complementary to aptamer-O and aptamer-A (denoted as probe-O and probe-A) were modified on the surface of MNPs through the formation of peptide bonds (Table S1, Supporting Information).[3,44] The carboxyl groups of MNPs were first activated through 100 μM EDC and 10 μM sulfo-NHS overnight. An aliquot of 10 μL of 500 nM MNPs, 2.5 μL of 100 μM probe-O, and 2.5 μL of 100 μM probe-A were added into 1 mL of pH 7.4 PBS buffer solution. The mixtures were incubated for 10 h under shaking at room temperature. The ratio of DNA to MNPs was optimized to 100:1. Probe−MNP conjugations were washed with ethanol three times and then were dissolved in 500 μL of ultrapure water.

2.5. SERS Signal Dependent Double Detection of OTA and AFB1. An amount of 20 μL of 10 nM probes−MNPs, 20 μL of 200 nM aptamer-O-Ag@4-ATP@Au CS NPs, 20 μL of 200 nM aptamer-A-Ag@4-NTP@Au CS NPs, OTA, and AFB1 were mixed in 100 μL of Tris·HCl buffer. The mixtures were incubated at 40 °C for 2 h to ensure complete recognition between aptamers and mycotoxins. MNPs-Ag@Au CS NPs core−satellite assemblies were purified through magnetic separation and dissolved in 100 μL of ultrapure water. SERS spectra of assemblies were measured through Raman spectrometer with a 785 nm Ar^+ ion laser source at room temperature, to avoid plasmon dephasing associated with the interband transition of Au at 2.5 eV (~500 nm).[45,46] The baselines of the SERS spectra in all the figures were processed by the open source RamanCooker software.

2.6. Specificity and Reproducibility. The specificity of Raman aptasensors was studied in the presence of 20 ng/mL OTB, OTC, warfarin, AFB2, AFG1, AFG2, FB1, L-Cys, BSA, GSH, and the control groups without any targets. The reproducibility of the substrates was

DOI: 10.1021/acsami.5b07804
ACS Appl. Mater. Interfaces 2015, 7, 21780−21786

investigated at different concentrations of OTA and AFB1. Mycotoxins were spiked into negative maize meal which was sterilized in an autoclave. The mixtures were dissolved in 1 mL of 50% methanol−water solution, and then were filtrated three times to remove the precipitates. The filtrate was collected and the SERS spectra were measured by the same detection procedures. For the detection of real samples, the samples should be first diluted to several concentrations, and then were detected by the developed Raman aptasensors.

3. RESULTS AND DISCUSSION

3.1. Principle of SERS Signal Based Double Detection of Mycotoxins. A schematic diagram illustrates the mechanism of the proposed Raman aptasensors (Scheme 1). SERS

Scheme 1. Schematic Illustration of Double Detection of OTA and AFB1 with the Use of SERS Labels Embedded Ag@Au CS NPs

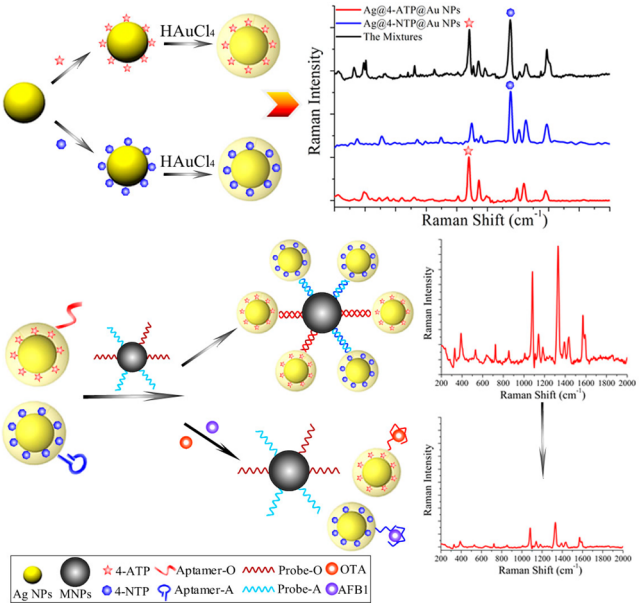

tags are fabricated by embedding 4-NTP or 4-ATP in the junction of Ag core and Au shell. Aptamer-O and aptamer-A are modified on the surface of Ag@4-ATP@Au CS NPs and Ag@4-NTP@Au NPs, respectively. Under optimized condition, probe functionalized MNPs would capture several SERS tags through the hybridization reaction between aptamers and probes, resulting in the formation of SERS-active MNPs-Ag@Au CS NPs core−satellite assemblies. In the presence of OTA and AFB1, targets and probes on MNPs would competitively combine with the aptamers SERS tags, inducing the dissociation of each Ag@Au CS NPs from MNPs and further decreasing the SERS signal. There is a linear relationship between the concentration of mycotoxins and SERS intensity.

3.2. Preparation and Characterization of SERS Labels Embedded Ag@Au CS NPs. The preparation of solid Ag@Au CS NPs is critical to amplify the SERS signal of Raman labels in the junction. The syntheses of solid Ag@Au CS NPs were attempted by the depositing of $HAuCl_4$ solution on Ag NPs (Figure 1 and Figure S1, Supporting Information). It was reported that hollow Ag@Au NPs were easily produced due to the galvanic replacement.[39,40,45] Adjusting the pH to 9.5 could ultimately suppress the galvanic reaction. This is because the reduction power of ascorbic acid could be greatly enhanced at pH 9.5, and $HAuCl_4$ was exclusively reduced before it could

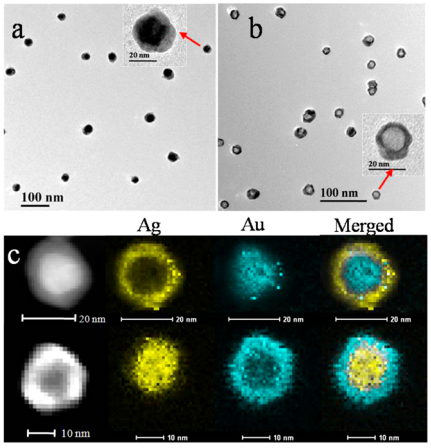

Figure 1. TEM images of Au@Ag CS NPs (a) and Ag@Au CS NPs (b) and their corresponding HAADF-STEM-EDS. The yellow and turquoise colors represent Ag element and Au element.

participate in the galvanic reaction with Ag NPs.[45] As shown in Figure 1, solid Ag@Au CS NPs covered by 4.5 ± 1.0 nm Au shell are synthesized. Au@Ag CS NPs are also prepared by depositing $AgNO_3$ solution on Au NPs, in order to compare the SERS activity of Ag@Au CS NPs and Au@Ag CS NPs. As shown in Figure 1, TEM images exhibit a complete contrast between Au and Ag. High angle annular dark field scanning transmission electron microscopy energy dispersive spectrometry (HAADF-STEM-EDS) was applied to characterize the detailed structures of CS NPs (Figure 1c). Au@Ag CS NPs are composed of Au core and Ag shell. Excitingly, Ag@Au CS NPs show solid structures which are composed by Ag core and Au shell.

Tuning of the nano-object size, shape, and composition alters the LSPR spectral position and amplitude. The behavior of the LSPR peak is markedly different for the CS NPs depending on the coupling mode of the plasmons.[25,42,47] Ag NPs exhibit an LSPR peak at 401 nm. A characteristic LSPR peak of Ag@Au CS NPs displays a 165 nm red shift. A blue shift of the LSPR from 519 to 399 nm is observed for Au NPs after the deposition of Ag shell (Figure 2a).[42,47] Clear evidence of shell-dependent plasmonic coupling prompts us to consider potential SERS activity of SERS labels embedded Ag@Au CS NPs. In comparison to pure 4-ATP, a slight enhancement of SERS intensity is observed for 4-ATP attached Au NPs or Ag NPs, while a drastically increased SERS signal occurs for SERS labels embedded CS NPs (Figure 2b). In particular, SERS signal of Ag@4-ATP@Au CS NPs is about 2 orders of magnitude stronger than that of Au@4-ATP@Ag CS NPs. The amplification of SERS signal for Ag@4-ATP@Au CS NPs can be summarized as follows: (a) the strongest fascinating LSPR of Ag core is essential to the enhancement of SERS signal,[48] (b) the external Au shell endows NPs with excellent chemical stability, (c) the plasmonic coupling effect at the tight junction of Ag core and Au shell induces enormous electromagnetic enhancement,[37] and (d) the intimate interaction between Raman labels and the plasmonic structure is critical for the generation of electromagnetic field.[29] SERS labels embedded Ag@Au CS NPs exhibit thermal and chemical stability when exposed to ambient light for 28 days and suffer from different temperatures (Figure S2, Supporting Information). The Au shell prevents the SERS labels from leaching out into the medium, but protects the Ag core from the susceptibility of

DOI: 10.1021/acsami.5b07804
ACS Appl. Mater. Interfaces 2015, 7, 21780−21786

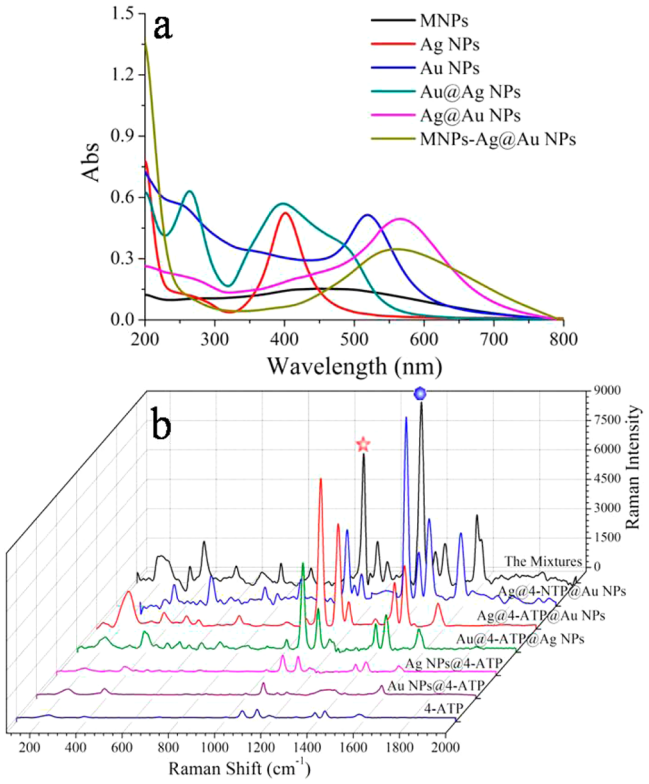

Figure 2. (a) UV−vis spectra of MNPs, Ag NPs, Au NPs, Au@Ag CS NPs, Ag@Au CS NPs, and MNPs-Ag@Au CS NPs core−satellite assemblies. (b) SERS spectra of 4-ATP, 4-ATP modified Au NPs and Ag NPs, Au@4-ATP@Ag CS NPs, Ag@4-ATP@Au CS NPs, Ag@4-NTP@Au CS NPs, and the mixtures of Ag@4-ATP@Au CS NPs and Ag@4-NTP@Au CS NPs.

oxidation.[29] The combination of excellent SERS activity and chemical stability enables SERS labels embedded Ag@Au CS NPs to be an alternative candidate for a variety of sensitive detection applications.

Distinct representative Raman labels could be applied to conveniently fabricate promising multiple SERS labels embedded Ag@Au CS NPs. As illustrated in Figure 2b, Ag@4-NTP@Au CS NPs are also fabricated and exhibit unique SERS spectra with minimal spectral overlapping in contrast to that of Ag@4-ATP@Au CS NPs.[38] Ag@4-ATP@Au CS NPs and Ag@4-NTP@Au CS NPs can be separately employed as the characterized peaks for the double detection of OTA and AFB1. SERS tags functionalized with aptamers show higher hydrodynamic sizes that increase from 27.4 ± 1.4 nm to 28.2 ± 1.8 nm (Figure S3a, Supporting Information).

3.3. Characterization of MNPs and MNPs-Ag@Au CS NPs Core−Satellite Assemblies. MNPs with strong magnetic response play a key role for the magnetic separation and the accuracy of method. As demonstrated in Figure 3, the size of MNPs is 240 ± 12 nm. MNPs can be completely separated from the disperse medium within 30 s under magnetic field. Probe-O and probe-A are modified on the surface of MNPs. The amounts of probe-O and probe-A on MNPs are almost similar due to the identical concentration and the same number of base pairs.[49] The hydrodynamic sizes of MNPs increase from 252.4 ± 9.6 nm to 254.8 ± 11.3 nm after the modification of probes (Figure S3b, Supporting Information).

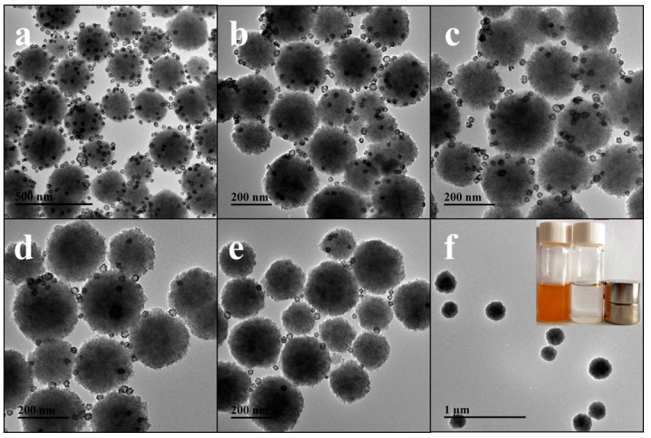

Figure 3. (a−e) TEM images of MNPs-Ag@Au CS NPs core−satellite assemblies in the presence of different concentrations of mycotoxins: (a) 0 ng/mL OTA and 0 ng/mL AFB1; (b) 0.10 ng/mL OTA and 0.50 ng/mL AFB1; (c) 1.00 ng/mL OTA and 5.00 ng/mL AFB1; (d) 10.00 ng/mL OTA and 50.00 ng/mL AFB1; (e) 100.00 ng/mL OTA and 500.00 ng/mL AFB1. (f) TEM images of MNPs. (inset) Photograph of MNPs solution before and after magnetic separation.

MNPs-Ag@Au CS NPs core−satellite assemblies are prepared depending on the hybridization between probes and aptamers. The high amount of probes induces the attachment of more aptamers-Ag@Au CS NPs on MNPs. The average number of Ag@Au CS NPs around MNPs is statistically analyzed to 36 ± 5 (Figure 3a and Figure S4, Supporting Information). An LSPR feature at 566 nm is observed for assemblies, which is essentially identical to that of Au@Ag CS NPs (Figure 2a). In comparison to the assemblies prepared by "bare" NPs, the fabricated MNPs-Ag@Au CS NPs core−satellite assemblies exhibit strong SERS signal after magnetic separation (Figure S5, Supporting Information).

3.4. Double-Analyte Raman Aptasensors. SERS labels embedded Ag@Au CS NPs produce quantitative SERS signal without the precise control of the gap size between neighboring NPs. There are no obvious changes for the SERS signal between monodisperse and small aggregated Ag@Au CS NPs (Figure S6, Supporting Information). The hot spots in aggregated Ag@Au CS NPs on MNPs have little effect on the quantitative SERS achievement. The fabricated MNPs-Ag@Au CS NPs core−satellite assemblies show potential application for the detection of multiple mycotoxins which possess different lengths of aptamers.

Considering the position and intensity of the fabricated SERS tags as well as the easy distinction from each other, the Raman peak at 1076 cm^{-1} shows the strongest intensity and is chosen as the identification position for the quantitative analysis of OTA, while the strongest peak at 1335 cm^{-1} is regarded as the characteristic signal for AFB1 detection. In the presence of OTA and AFB1, the high specific response of aptamers toward targets induces a structural switch of aptamers and the dissociation of SERS tags from MNPs (Figure 3a−e). The residual MNPs-Ag@Au CS NPs assemblies are completely separated under a magnetic field, and there are only dissociated Ag@Au CS NPs in the disperse medium (Figure S7, Supporting Information). With the increasing concentration of mycotoxins, the number of Ag@Au CS NPs on MNPs decreases from 36 ± 5 to 2 ± 1, and the hydrodynamic sizes decrease from 330.8 ± 14.9 nm to 252.4 ± 9.6 nm (Figure S4b, Supporting Information).

DOI: 10.1021/acsami.5b07804
ACS Appl. Mater. Interfaces 2015, 7, 21780−21786

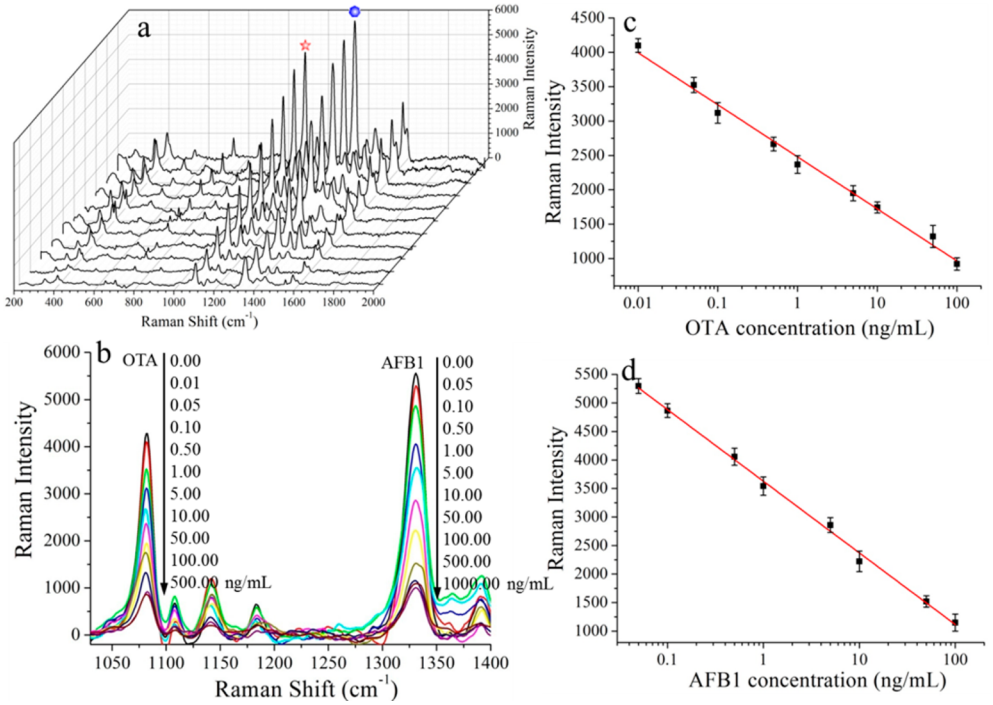

Figure 4. (a) SERS spectra of SERS labels embedded Ag@Au CS NPs for double detection of OTA and AFB1. (b) Enlarged SERS spectra of SERS tags at different concentrations of OTA and AFB1. (c, d) Standard curves between Raman signal of assemblies and concentration of mycotoxins.

SERS peak at 1076 cm^{-1} for Ag@4-ATP@Au CS NPs decreases with the increase in concentration of OTA from 0.01 to 100 ng/mL (Figure 4). The identification of aptamers is saturated at higher concentration of OTA. A standard curve between SERS intensity at 1076 cm^{-1} and OTA concentration is established with a good correlation (R^2 = 0.9916, Figure 4c). The LOD is calculated to be 0.006 ng/mL for OTA based on 3σ criterion. Similarly, a drastically decreased SERS signal at 1335 cm^{-1} is observed with the increasing concentration of AFB1 from 0.05 to 100 ng/mL. No obvious changes of SERS signal are observed among 100, 500, and 1000 ng/mL AFB1. A standard curve between SERS intensity at 1335 cm^{-1} for Ag@4-NTP@Au CS NPs and AFB1 concentration is established with a good correlation in the range 0.05−100 ng/mL (R^2 = 0.9956, Figure 4d). The LOD is calculated to be 0.03 ng/mL for AFB1. The disparity in the LOD values of the various mycotoxins is determined by the different binding constants of the aptamers. The combination of specific aptasensors and excellent SERS capabilities of each individual SERS labels embedded CS NP achieves sensitive DNA-amplification-free double mycotoxin detection (Table 1).

3.5. Selectivity Evaluation and Analytical Application. The selectivity of Raman aptasensors is investigated in the presence of nonspecific molecules, involving OTB, OTC, warfarin, AFB2, AFG1, AFG2, FB1, L-Cys, BSA, GSH, and the control groups without any targets (Table S2, Supporting Information). As illustrated in Figure S8, SERS signal shows no obvious changes for nonspecific molecules, but exhibits a significant decrement at 1335 cm^{-1} in the presence of AFB1. SERS intensity at 1076 cm^{-1} for 20 ng/mL OTA is 2.9-fold lower than that of 0 ng/mL OTA, but remains unchanged at 1335 cm^{-1}. There is almost no cross-reaction between AFB1 and OTA, owing to the favorable bioaffinity of aptamers.

The analysis of spiked samples with the developed Raman aptasensors is considered. Raman aptasensors exhibit sensitive SERS response in the presence of OTA and AFB1 with various concentration ratios (Figure S9, Tables S3 and S4, Supporting Information). A progressive decrease occurs with the increasing amount of mycotoxins. The measured SERS signal is well-fitted with the established calibration curve. The spiked samples are further quantified by a classic HPLC method. The results obtained with Raman aptasensors show good correlation with those obtained by HPLC (Table S3, Supporting Information). The recovery rates are calculated in the ranges of 95.00 ± 3.08% to 99.48 ± 3.79% for OTA and 95.00 ± 3.35% to 99.65 ± 3.95% for AFB1. The relative standard deviation of this method is within 3.95%. The results indicate that SERS embedded Ag@Au CS NPs would be the potential and reproducible SERS tags for multiple screening OTA and AFB1 residues in maize meal.

4. CONCLUSIONS

In summary, an accurate and sensitive SERS tags driven double detection of OTA and AFB1 is established for the first time. The prepared SERS labels embedded Ag@Au CS NPs not only possess thermal and chemical stability, but exhibit amplified SERS signal originating from the plasmonic coupling at the junction between Ag core and Au shell. Two kinds of SERS tags are applied for the rapid and sensitive detection of OTA and AFB1 in maize meal, without the aid of nucleic acid amplification strategies. The easy-to-operate embedded protocol could be extended to explore a large set of SERS tags for simultaneous screening of other illegal hazardous substances.

■ ASSOCIATED CONTENT

Supporting Information

The Supporting Information is available free of charge on the ACS Publications website at DOI: 10.1021/acsami.5b07804.

Calculation of LODs; TEM images of Au NPs, Ag NPs, Ag@Au CS NPs, and assemblies; Raman spectra of Ag@

DOI: 10.1021/acsami.5b07804
ACS Appl. Mater. Interfaces 2015, 7, 21780−21786

Au CS NPs when exposed to light and temperatures; DLS data of DNA−NP conjugations and assemblies; statistical analysis of number of Ag@Au CS NPs on MNPs; SERS spectra of aggregated and monodisperse Ag@Au CS NPs; Raman response of the sensor in the presence of different targets; tables showing detailed sequences of aptamers, structures of mycotoxins, and recoveries of mycotoxins (PDF)

AUTHOR INFORMATION

Corresponding Authors

*E-mail: zhaoyuan@jiangnan.edu.cn (Y.Z.).
*E-mail: qsong@jiangnan.edu.cn (Q.S.).

Notes

The authors declare no competing financial interest.

ACKNOWLEDGMENTS

This work is financially supported by the National Natural Science Foundation of China (21403090, 21175060), the China Postdoctoral Science Foundation (2015M570405), the Fundamental Research Funds for the Central Universities (No. JUSRP11424), and the Ministry of Education (MOE) and State Administration of Foreign Experts Affairs (SAFEA) for the 111 Project (B13025).

REFERENCES

(1) Yue, S.; Jie, X.; Wei, L.; Bin, C.; Dou Dou, W.; Yi, Y.; QingXia, L.; JianLin, L.; TieSong, Z. Simultaneous detection of ochratoxin A and fumonisin B1 in cereal samples using an aptamer-photonic crystal encoded suspension array. *Anal. Chem.* **2014**, *86*, 11797−11802.

(2) Wang, D.; Hu, W.; Xiong, Y.; Xu, Y.; Li, C. M. Multifunctionalized reduced graphene oxide-doped polypyrrole/pyrrolepropylic acid nanocomposite impedimetric immunosensor to ultrasensitively detect small molecular aflatoxin B1. *Biosens. Bioelectron.* **2015**, *63*, 185−189.

(3) Zhao, Y.; Luo, Y.; Li, T.; Song, Q. Au NPs driven electrochemiluminescence aptasensors for sensitive detection of fumonisin B1. *RSC Adv.* **2014**, *4*, 57709−57714.

(4) Beloglazova, N. V.; Speranskaya, E. S.; Wu, A.; Wang, Z.; Sanders, M.; Goftman, V. V.; Zhang, D.; Goryacheva, I. Y.; De Saeger, S. Novel multiplex fluorescent immunoassays based on quantum dot nanolabels for mycotoxins determination. *Biosens. Bioelectron.* **2014**, *62*, 59−65.

(5) Park, J. H.; Byun, J. Y.; Mun, H.; Shim, W. B.; Shin, Y. B.; Li, T.; Kim, M. G. A regeneratable, label-free, localized surface plasmon resonance (LSPR) aptasensor for the detection of ochratoxin A. *Biosens. Bioelectron.* **2014**, *59*, 321−327.

(6) Shim, W. B.; Kim, M. J.; Mun, H.; Kim, M. G. An aptamer-based dipstick assay for the rapid and simple detection of aflatoxin B1. *Biosens. Bioelectron.* **2014**, *62*, 288−294.

(7) Shim, W.-B.; Mun, H.; Joung, H.-A.; Ofori, J. A.; Chung, D.-H.; Kim, M.-G. Chemiluminescence competitive aptamer assay for the detection of aflatoxin B1 in corn samples. *Food Control* **2014**, *36*, 30−35.

(8) Huang, L.; Wu, J.; Zheng, L.; Qian, H.; Xue, F.; Wu, Y.; Pan, D.; Adeloju, S. B.; Chen, W. Rolling chain amplification based signal-enhanced electrochemical aptasensor for ultrasensitive detection of ochratoxin A. *Anal. Chem.* **2013**, *85*, 10842−10849.

(9) Ma, W.; Yin, H.; Xu, L.; Xu, Z.; Kuang, H.; Wang, L.; Xu, C. Femtogram ultrasensitive aptasensor for the detection of Ochratoxin A. *Biosens. Bioelectron.* **2013**, *42*, 545−549.

(10) Guo, X.; Wen, F.; Zheng, N.; Luo, Q.; Wang, H.; Wang, H.; Li, S.; Wang, J. Development of an ultrasensitive aptasensor for the detection of aflatoxin B1. *Biosens. Bioelectron.* **2014**, *56*, 340−344.

(11) Cruz-Aguado, J. A.; Penner, G. Fluorescence Polarization Based Displacement Assay for the Determination of Small Molecules with Aptamers. *Anal. Chem.* **2008**, *80*, 8853−8855.

(12) Chen, J.; Zhang, X.; Cai, S.; Wu, D.; Chen, M.; Wang, S.; Zhang, J. A fluorescent aptasensor based on DNA-scaffolded silver-nanocluster for ochratoxin A detection. *Biosens. Bioelectron.* **2014**, *57*, 226−231.

(13) Wang, R.; Xiang, Y.; Zhou, X.; Liu, L. H.; Shi, H. A reusable aptamer-based evanescent wave all-fiber biosensor for highly sensitive detection of Ochratoxin A. *Biosens. Bioelectron.* **2015**, *66*, 11−18.

(14) Ganbold, E.-O.; Lee, C. M.; Cho, E.-M.; Son, S. J.; Kim, S.; Joo, S.-W.; Yang, S. I. Subnanomolar detection of ochratoxin A using aptamer-attached silver nanoparticles and surface-enhanced Raman scattering. *Anal. Methods* **2014**, *6*, 3573−3577.

(15) Xie, S.; Chai, Y.; Yuan, Y.; Bai, L.; Yuan, R. Development of an electrochemical method for Ochratoxin A detection based on aptamer and loop-mediated isothermal amplification. *Biosens. Bioelectron.* **2014**, *55*, 324−329.

(16) Yang, M.; Jiang, B.; Xie, J.; Xiang, Y.; Yuan, R.; Chai, Y. Electrochemiluminescence recovery-based aptasensor for sensitive Ochratoxin A detection via exonuclease-catalyzed target recycling amplification. *Talanta* **2014**, *125*, 45−50.

(17) Zhang, R.; Zhang, Y.; Dong, Z. C.; Jiang, S.; Zhang, C.; Chen, L. G.; Zhang, L.; Liao, Y.; Aizpurua, J.; Luo, Y.; Yang, J. L.; Hou, J. G. Chemical mapping of a single molecule by plasmon-enhanced Raman scattering. *Nature* **2013**, *498*, 82−86.

(18) Li, J.-M.; Wei, C.; Ma, W.-F.; An, Q.; Guo, J.; Hu, J.; Wang, C.-C. Multiplexed SERS detection of DNA targets in a sandwich-hybridization assay using SERS-encoded core−shell nanospheres. *J. Mater. Chem.* **2012**, *22*, 12100−12106.

(19) Guarrotxena, N.; Bazan, G. C. Antitags: SERS-encoded nanoparticle assemblies that enable single-spot multiplex protein detection. *Adv. Mater.* **2014**, *26*, 1941−1946.

(20) Fabris, L.; Schierhorn, M.; Moskovits, M.; Bazan, G. C. Aptatag-based multiplexed assay for protein detection by surface-enhanced Raman spectroscopy. *Small* **2010**, *6*, 1550−1557.

(21) Zhao, Y.; Xu, L.; Liz-Marzán, L. M.; Kuang, H.; Ma, W.; Asenjo-García, A.; García de Abajo, F. J.; Kotov, N. A.; Wang, L.; Xu, C. Alternating Plasmonic Nanoparticle Heterochains Made by Polymerase Chain Reaction and Their Optical Properties. *J. Phys. Chem. Lett.* **2013**, *4*, 641−647.

(22) Xu, L.; Yan, W.; Ma, W.; Kuang, H.; Wu, X.; Liu, L.; Zhao, Y.; Wang, L.; Xu, C. SERS Encoded Silver Pyramids for Attomolar Detection of Multiplexed Disease Biomarkers. *Adv. Mater.* **2015**, *27*, 1706−1711.

(23) Zheng, Y. H.; Thai, T.; Reineck, P.; Qiu, L.; Guo, Y. M.; Bach, U. DNA-Directed Self-Assembly of Core-Satellite Plasmonic Nanostructures: A Highly Sensitive and Reproducible Near-IR SERS Sensor. *Adv. Funct. Mater.* **2013**, *23*, 1519−1526.

(24) Li, S.; Xu, L.; Ma, W.; Kuang, H.; Wang, L.; Xu, C. Triple Raman Label-Encoded Gold Nanoparticle Trimers for Simultaneous Heavy Metal Ion Detection. *Small* **2015**, *11*, 3435−3439.

(25) Lee, J. H.; Nam, J. M.; Jeon, K. S.; Lim, D. K.; Kim, H.; Kwon, S.; Lee, H.; Suh, Y. D. Tuning and Maximizing the Single-Molecule Surface-Enhanced Raman Scattering from DNA-Tethered Nanodumbbells. *ACS Nano* **2012**, *6*, 9574−9584.

(26) Zhao, Y.; Xu, L.; Liz-Marzán, L. M.; Kuang, H.; Ma, W.; Asenjo-García, A.; García de Abajo, F. J.; Kotov, N. A.; Wang, L.; Xu, C. Alternating Plasmonic Nanoparticle Heterochains Made by Polymerase Chain Reaction and Their Optical Properties. *J. Phys. Chem. Lett.* **2013**, *4*, 641−647.

(27) Evtugyn, G.; Porfireva, A.; Stepanova, V.; Sitdikov, R.; Stoikov, I.; Nikolelis, D.; Hianik, T. Electrochemical Aptasensor Based on Polycarboxylic Macrocycle Modified with Neutral Red for Aflatoxin B1 Detection. *Electroanalysis* **2014**, *26*, 2100−2109.

(28) Wang, Y.; Yan, B.; Chen, L. SERS tags: novel optical nanoprobes for bioanalysis. *Chem. Rev.* **2013**, *113*, 1391−1428.

(29) Mir-Simon, B.; Reche-Perez, I.; Guerrini, L.; Pazos-Perez, N.; Alvarez-Puebla, R. A. Universal One-Pot and Scalable Synthesis of SERS Encoded Nanoparticles. *Chem. Mater.* **2015**, *27*, 950−958.

(30) Shanthil, M.; Thomas, R.; Swathi, R.; George Thomas, K. Ag@SiO2 Core−Shell Nanostructures: Distance-Dependent Plasmon

DOI: 10.1021/acsami.5b07804
ACS Appl. Mater. Interfaces 2015, 7, 21780−21786

Coupling and SERS Investigation. *J. Phys. Chem. Lett.* **2012**, *3*, 1459−1464.
(31) Jun, B. H.; Noh, M. S.; Kim, G.; Kang, H.; Kim, J. H.; Chung, W. J.; Kim, M. S.; Kim, Y. K.; Cho, M. H.; Jeong, D. H.; Lee, Y. S. Protein separation and identification using magnetic beads encoded with surface-enhanced Raman spectroscopy. *Anal. Biochem.* **2009**, *391*, 24−30.
(32) Jun, B. H.; Noh, M. S.; Kim, J.; Kim, G.; Kang, H.; Kim, M. S.; Seo, Y. T.; Baek, J.; Kim, J. H.; Park, J.; Kim, S.; Kim, Y. K.; Hyeon, T.; Cho, M. H.; Jeong, D. H.; Lee, Y. S. Multifunctional silver-embedded magnetic nanoparticles as SERS nanoprobes and their applications. *Small* **2010**, *6*, 119−125.
(33) Li, X.; Wang, L.; Li, C. Rolling-circle amplification detection of thrombin using surface-enhanced Raman spectroscopy with core-shell nanoparticle probe. *Chem. - Eur. J.* **2015**, *21*, 6817−6822.
(34) Zhang, X.; Zhu, Y.; Yang, X.; Zhou, Y.; Yao, Y.; Li, C. Multifunctional Fe_3O_4@TiO_2@Au magnetic microspheres as recyclable substrates for surface-enhanced Raman scattering. *Nanoscale* **2014**, *6*, 5971−5979.
(35) Hong, S.; Acapulco, J. A. I.; Jang, H. Y.; Park, S. Au Nanodisk-Core Multishell Nanoparticles: Synthetic Method for Controlling Number of Shells and Intershell Distance. *Chem. Mater.* **2014**, *26*, 3618−3623.
(36) Singh, D. K.; Ganbold, E. O.; Cho, E. M.; Cho, K. H.; Kim, D.; Choo, J.; Kim, S.; Lee, C. M.; Yang, S. I.; Joo, S. W. Detection of the mycotoxin citrinin using silver substrates and Raman spectroscopy. *J. Hazard. Mater.* **2014**, *265*, 89−95.
(37) Feng, Y.; Wang, Y.; Wang, H.; Chen, T.; Tay, Y. Y.; Yao, L.; Yan, Q.; Li, S.; Chen, H. Engineering "hot" nanoparticles for surface-enhanced Raman scattering by embedding reporter molecules in metal layers. *Small* **2012**, *8*, 246−251.
(38) Zhao, Y.; Liu, L.; Kuang, H.; Wang, L.; Xu, C. SERS-active Ag@Au core−shell NP assemblies for DNA detection. *RSC Adv.* **2014**, *4*, 56052−56056.
(39) Hong, X.; Wang, D.; Cai, S.; Rong, H.; Li, Y. Single-crystalline octahedral Au-Ag nanoframes. *J. Am. Chem. Soc.* **2012**, *134*, 18165−18168.
(40) McEachran, M.; Keogh, D.; Pietrobon, B.; Cathcart, N.; Gourevich, I.; Coombs, N.; Kitaev, V. Ultrathin gold nanoframes through surfactant-free templating of faceted pentagonal silver nanoparticles. *J. Am. Chem. Soc.* **2011**, *133*, 8066−8069.
(41) Liu, Z.; Yang, Z.; Peng, B.; Cao, C.; Zhang, C.; You, H.; Xiong, Q.; Li, Z.; Fang, J. Highly sensitive, uniform, and reproducible surface-enhanced Raman spectroscopy from hollow Au-Ag alloy nanourchins. *Adv. Mater.* **2014**, *26*, 2431−2439.
(42) Zhao, Y.; Xu, L.; Ma, W.; Wang, L.; Kuang, H.; Xu, C.; Kotov, N. A. Shell-engineered chiroplasmonic assemblies of nanoparticles for zeptomolar DNA detection. *Nano Lett.* **2014**, *14*, 3908−3913.
(43) Zhao, Y.; Hao, C.; Yong, Q.; Qu, C.; Chen, W.; Peng, C.; Kuang, H.; Zhou, H.; Wang, L.; Xu, C. Systematic comparisons of genetically modified organism DNA separation and purification by various functional magnetic nanoparticles. *Int. J. Food Sci. Technol.* **2012**, *47*, 910−917.
(44) Zhao, Y.; Hao, C.; Ma, W.; Yong, Q.; Yan, W.; Kuang, H.; Wang, L.; Xu, C. Magnetic Bead-Based Multiplex DNA Sequence Detection of Genetically Modified Organisms Using Quantum Dot-Encoded Silicon Dioxide Nanoparticles. *J. Phys. Chem. C* **2011**, *115*, 20134−20140.
(45) Yang, Y.; Liu, J.; Fu, Z. W.; Qin, D. Galvanic replacement-free deposition of Au on Ag for core-shell nanocubes with enhanced chemical stability and SERS activity. *J. Am. Chem. Soc.* **2014**, *136*, 8153−8156.
(46) Rycenga, M.; Hou, K. K.; Cobley, C. M.; Schwartz, A. G.; Camargo, P. H. C.; Xia, Y. N. Probing the surface-enhanced Raman scattering properties of Au-Ag nanocages at two different excitation wavelengths. *Phys. Chem. Chem. Phys.* **2009**, *11*, 5903−5908.
(47) Zhao, Y.; Xu, L.; Ma, W.; Liu, L.; Wang, L.; Kuang, H.; Xu, C. Shell-programmed Au nanoparticle heterodimers with customized chiroptical activity. *Small* **2014**, *10*, 4770−4777.
(48) Garcia-Leis, A.; Garcia-Ramos, J. V.; Sanchez-Cortes, S. Silver Nanostars with High SERS Performance. *J. Phys. Chem. C* **2013**, *117*, 7791−7795.
(49) Maye, M. M.; Nykypanchuk, D.; Cuisinier, M.; van der Lelie, D.; Gang, O. Stepwise surface encoding for high-throughput assembly of nanoclusters. *Nat. Mater.* **2009**, *8*, 388−391.
(50) Wu, X.; Gao, S.; Wang, J. S.; Wang, H.; Huang, Y. W.; Zhao, Y. The surface-enhanced Raman spectra of aflatoxins: spectral analysis, density functional theory calculation, detection and differentiation. *Analyst* **2012**, *137*, 4226−4234.
(51) Lee, K. M.; Herrman, T. J.; Bisrat, Y.; Murray, S. C. Feasibility of surface-enhanced Raman spectroscopy for rapid detection of aflatoxins in maize. *J. Agric. Food Chem.* **2014**, *62*, 4466−4474.
(52) Ko, J.; Lee, C.; Choo, J. Highly sensitive SERS-based immunoassay of aflatoxin B1 using silica-encapsulated hollow gold nanoparticles. *J. Hazard. Mater.* **2015**, *285*, 11−17.

DOI: 10.1021/acsami.5b07804
ACS Appl. Mater. Interfaces 2015, 7, 21780−21786